AIMS Materials Science, 6(2): 288–300.
DOI: 10.3934/matersci.2019.2.288
Received: 25 December 2018
Accepted: 24 March 2019
Published: 08 April 2019

http://www.aimspress.com/journal/Materials

Research article

Effects of solution composition on corrosion behavior of 13 mass% Cr martensitic stainless steel in simulated oil and gas environments

Masatoshi Sakairi[1,*], Hirotaka Mizukami[2] and Shuji Hashizume[3]

[1] Faculty of Engineering, Hokkaido University, Kita-13, Nishi-8, Kita-ku, Sapporo, Hokkaido 060-8628, Japan
[2] Graduate School of Engineering, Hokkaido University, Kita-13, Nishi-8, Kita-ku, Sapporo, Hokkaido 060-8628, Japan (Presently INPEX, 30-23-9, Kita-karasuyama, Setagaya, Tokyo, 157-0061, Japan)
[3] TenarisNKKTubes, 1-10 Minamiwatarida, Kawasaki, Kanagawa 210-0855, Japan

*** Correspondence:** Email: msakairi@eng.hokudai.ac.jp; Tel: +81117067111; Fax: +81117067881.

Abstract: The effects of CH_3COONa and CO_2 on the corrosion behavior of 13 mass% Cr martensitic stainless steel in simulated oil and gas environments were investigated with electrochemical and surface analysis techniques. The electrochemical results showed that a plateau region and sudden increase in the current density of the anodic polarization curves. The current density of the plateau region decreased with increasing CH_3COONa concentrations. The pitting corrosion potential shifted to the positive direction with increasing CH_3COONa concentrations, and shifted to a negative value by adding CO_2. From the surface analysis, a Cr enriched layer had formed on the sample surface after immersion tests, and the thickness of this layer became thinner with increasing CH_3COONa concentration. The surface analysis results after the immersion tests suggested the presence of CH_3COO^- or HCO_3^- on the surface.

Keywords: 13 mass% Cr martensitic stainless steel; CH_3COONa; CO_2; XPS; GDS; oxide film structure

1. Introduction

Oil and gas fields are very severe environments for metals, and high corrosion resistance and strength steels are generally used. Stress corrosion cracking (SCC), sulfide stress cracking (SSC) and hydrogen embrittlement (HE) are principal corrosion problems of steels used in oil and gas environments. The corrosion behavior of steels has been examined in simulated oil and gas environments [1–16]. Kimura et al. reported that the modified 13 mass% Cr stainless steel showed excellent resistance to CO_2 corrosion and resistance to SSC [2]. Sunaba et al. investigated the effects of chloride ion concentration on the passive and corrosion product films of modified martensitic stainless steels at high temperatures in CO_2 environments [7]. They reported that molybdenum improved stability of the corrosion product films in high temperature CO_2 and the presence of chloride ions. Hashizume et al. introduced a solution flow type micro-droplet cell and a glow discharge optical emission spectrometer (GDS) to investigate the electrochemical behavior of low carbon 13 mass% Cr welded joints and the effect of a post welded heat treatment (PWHT) in oil and gas environments [17]. They reported that the PWHT eliminated the Cr depleted layer formed during welding, and reduced the SCC susceptibility.

Hashizume et al. also investigated the effects of chemical composition and tempering of martensitic stainless steel on corrosion rates and pitting potentials in simulated CO_2 gas wells [13]. They reported that the corrosion rate and the pitting potential in environments simulating CO_2 gas wells were governed mainly by the amount of Cr in the steel matrix. The effect of acetate ions on the structure of surface oxide films and corrosion behavior of 13 mass% Cr stainless steel in 25% NaCl solutions were investigated by X-ray photoelectron spectroscopy (XPS) and electrochemical techniques [18]. It was found that the intensity ratios of both $Fe^0/(Fe^{3+} + Fe^{2+} + Fe^0)$ and $Cr^0/(Cr^{3+} + Cr^0)$ decrease with increasing concentration of CH_3COONa, and after a minimum increased with further increasing in CH_3COONa concentration. Fierro et al. applied XPS for the analysis of the corrosion film formed on 13 mass% Cr martensitic stainless steel in CO_2-H_2S-Cl^- [19,20]. The presence of H_2S resulted in more the formation of the less protective Fe sulfide-rich and Fe oxide-rich layers, while the presence of CO_2 resulted in Cr oxide enrichment in the outermost layers of the film. Islam et al. investigated the corrosion layer on pipeline steel in CO_2 containing environments (sweet environments) [21].

However, the effects of environmental parameters such as pH, the concentration of CH_3COONa, and CO_2 on corrosion behavior of stainless steels have not been fully elucidated. The purpose of this study is to investigate the effects of the concentrations of CH_3COONa and CO_2 on the corrosion behavior of 13 mass% Cr martensitic stainless steels in simulated oil and gas environments.

2. Materials and method

2.1. Samples and preparation

Plates of 13 mass% Cr martensitic stainless steel (12.4 mass% Cr, 0.2 mass% C) with 3 mm thickness were used as samples. The sample size for electrochemical and XPS analysis was 7 × 15 mm, and for Fourier transform infrared spectroscopy (FT-IR) analysis was 15 × 15 mm.

For electrochemical measurement, Cu wires were soldered to the samples and then embedded in epoxy resin. The exposed surface of the embedded samples was ground with SiC abrasive paper from #240 to #1200 grit size. For immersion corrosion tests, samples were embedded in epoxy resin. The exposed surfaces of the samples were ground with SiC abrasive paper from #240 to #2400 grit size. The samples were ultrasonically cleaned in ethanol and in highly purified water, before the tests.

2.2. Solutions

Solutions of 5% NaCl with 0, 0.4, 4.0 g/L CH_3COONa were used as test solutions. The pH of the solutions was adjusted to 3.5 by HCl. Before the experiments, N_2 gas was bubbled through the solutions for 3.6 ks to reduce the concentration of dissolved O_2 as low as possible, and then CO_2 gas was bubbled as needed. The solution temperature was 353 K, and detailed procedures of the gas bubbling and pH adjustment are illustrated in Figure 1. During experiments, N_2 or CO_2 gas flowed over the solutions.

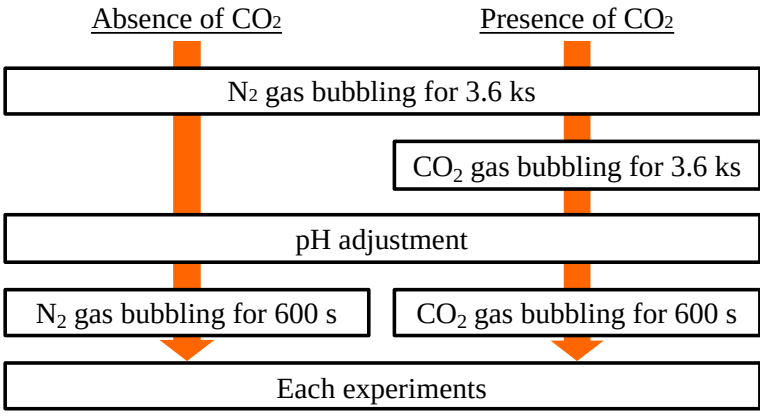

Figure 1. Schematic representation of the experimental procedure of this study.

2.3. Anodic potentiodynamic polarization measurement

Anodic potentiodynamic polarization measurements were carried out in a three electrode cell. A Pt plate and Ag/AgCl sat. KCl was used as counter and reference electrodes respectively. The samples were immersed in the solutions for 21.6 ks and measured the immersion potential, E_{im}, and then the polarization measurements with a scan rate of 0.5 mV/s were started from (E_{im} – 10) mV until current density reached 1 mA/cm^2. After the measurements, samples were rinsed with highly purified water and dried in a desiccator, and then the surface observations were performed with an optical microscope. Samples with crevice corrosion were discarded.

2.4. Immersion corrosion tests and surface analysis

The samples were immersed in the solutions for 21.6 ks. After the immersion, samples were

rinsed with highly purified water and dried in the desiccator. The sample surfaces were analyzed by XPS (JEOL Ltd., JPS-9200). For the XPS analysis, Mg Kα (1253.6 eV) was used as the X-ray source, and the analysis area was 1 × 1 mm. The XPS depth analysis was carried out by sputtering with Ar ions. The sputtering time was converted to depth by the sputtering rate of SiO_2. The wide range of depth profiles of Fe, Cr, and O were obtained by GDS (Horiba-Jobin Yvon, JY 5000 RF). The analysis area was 4 mm in diameter. The FT-IR (JASCO, FT-IR 4700) was used to determine the organic substances on the samples. The IR spectra were measured by reflection absorption spectroscopy (RAS) with the resolution of 1 cm^{-1}. The background spectra were obtained with gold evaporation mirror and the subtracted the obtained samples spectra. The surface observation was carried out with a scanning electron microscope, SEM (JEOL Ltd., JSL6510-LA).

3. Results and discussion

3.1. Anodic polarization curves

Anodic polarization curves were measured after 21.6 ks immersion and are shown in Figure 2. All curves except for 0 g/L CH_3COONa in the presence of CO_2 have the plateau region in the current, which implies that the corrosion reaction reaches a temporary steady state. The currents of plateau regions are higher than that of general passive current [22]. This result suggests that the passive state may not be achieved in the experimental conditions of this study. The current suddenly increased as the potential moves to a positive direction, which may imply the initiation of pitting corrosion. Hereafter, the plateau region in the current is called the average current density of the flat region, i_{flat}, and the potential at 1 mA/cm^2 is called pitting potential, E_{pit}.

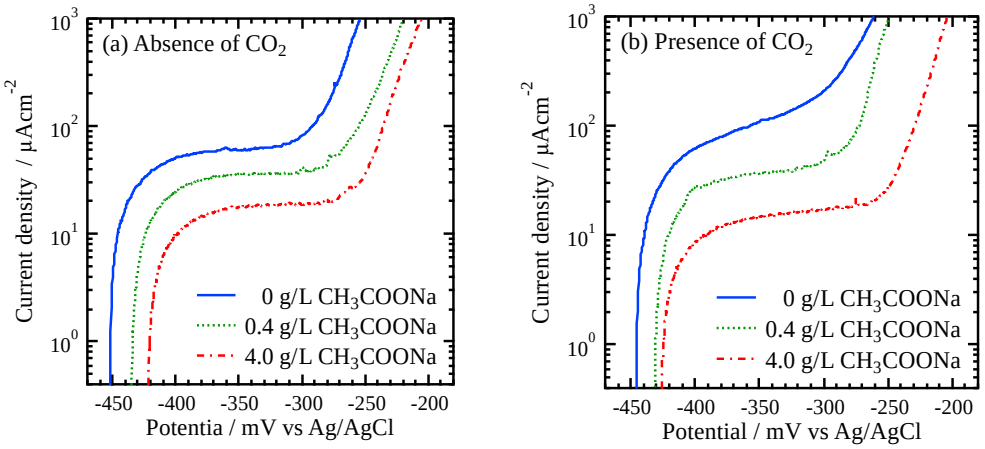

Figure 2. Anodic polarization curves after 21.6 ks immersion in solutions with (a) absence of CO_2 and (b) presence of CO_2.

The relationships between these two parameters, i_{flat} and E_{pit}, and the CH_3COONa concentration are shown in Figure 3. In Figure 3a, the i_{flat} decreases with increasing CH_3COONa concentration independent of CO_2 bubbling, implying that adding CH_3COONa inhibits the corrosion reaction. In Figure 3b, E_{pit} obtained in the solutions of the presence of CO_2 increases with increasing

CH_3COONa concentration, however, the effect of CH_3COONa addition is not significant in the solutions of an absence of CO_2.

The surface optical images of the samples after the polarization tests are shown in Figure 4. Dark spots which may be related to pitting corrosion are observed, and the number of the spot decreased with increasing concentration of CH_3COONa. This result coincides with Figure 3b.

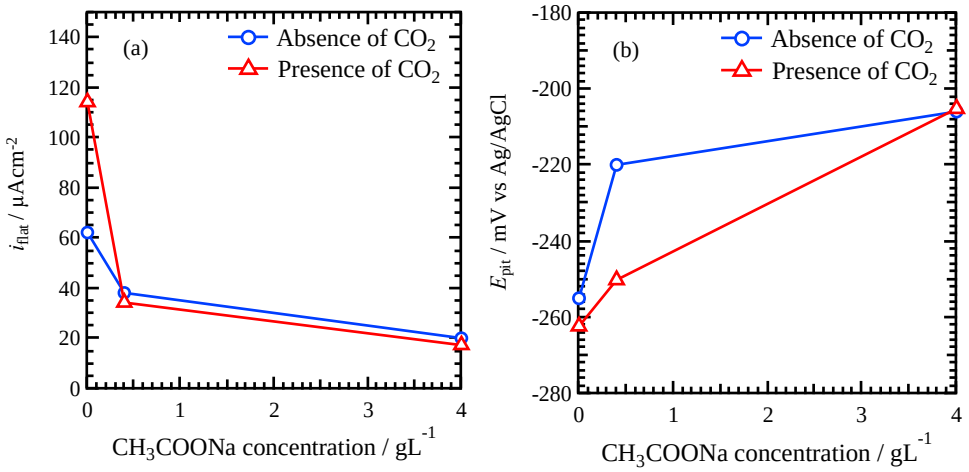

Figure 3. (a) i_{flat} and (b) E_{pit} as a function of CH_3COONa concentration.

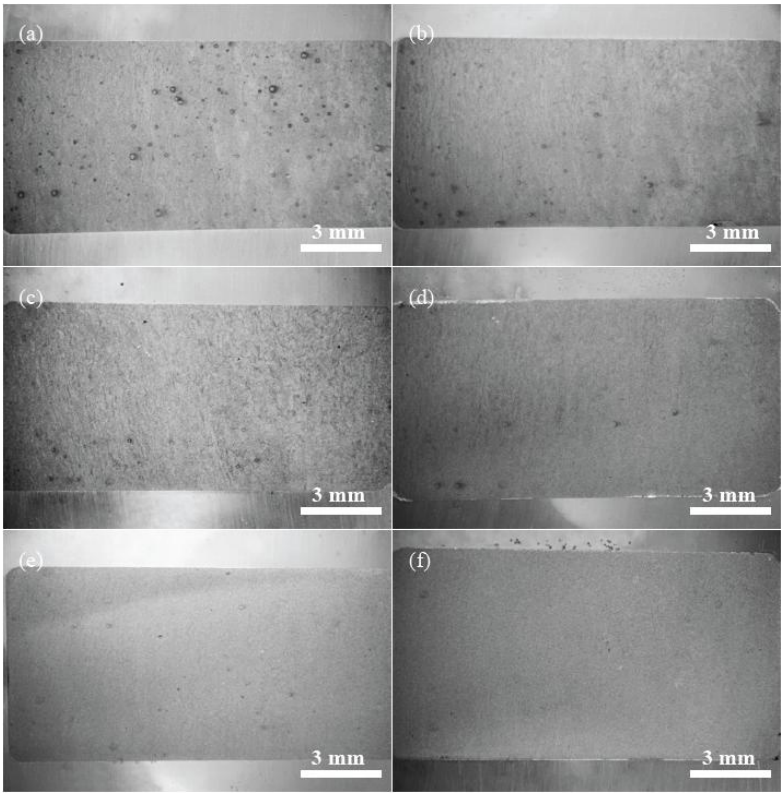

Figure 4. Surface images of samples after polarization tests. (a) and (b) 0 g/L CH_3COONa, (c) and (d) 0.4 g/L CH_3COONa, (e) and (f) 4.0 g/L CH_3COONa. (a), (c), (e) absence of CO_2; (b), (d), (f) presence of CO_2.

3.2. XPS spectra

The sample surfaces were examined by XPS after immersion in 4.0 g/L CH_3COONa absence of CO_2 for 21.6 ks. Figure 5 shows XPS narrow scan spectra of (a) Fe 2p3/2, (b) Cr 2p3/2, (c) O 1s, and (d) C 1s at different depths. In the narrow scan spectra of Fe 2p3/2 (Figure 5a), no peak is observed from 0 and 10 nm, while peaks around 707 eV are measured depth deeper than 10 nm. The peaks are attributed to Fe^{0+} [23–27], and the intensity of the peak increases with depth. In the narrow scan spectra of Cr 2p3/2 (Figure 5b), the peaks around 577 eV are observed depth from 0 nm to 70 nm. The peaks are attributed to Cr^{3+} [23,25–27], and the intensity decreases with depth. The peaks around 574 eV are appeared after sputtering. The peaks are attributed to Cr^{0+} [23,25–27], and the intensity of the peak increases with depth.

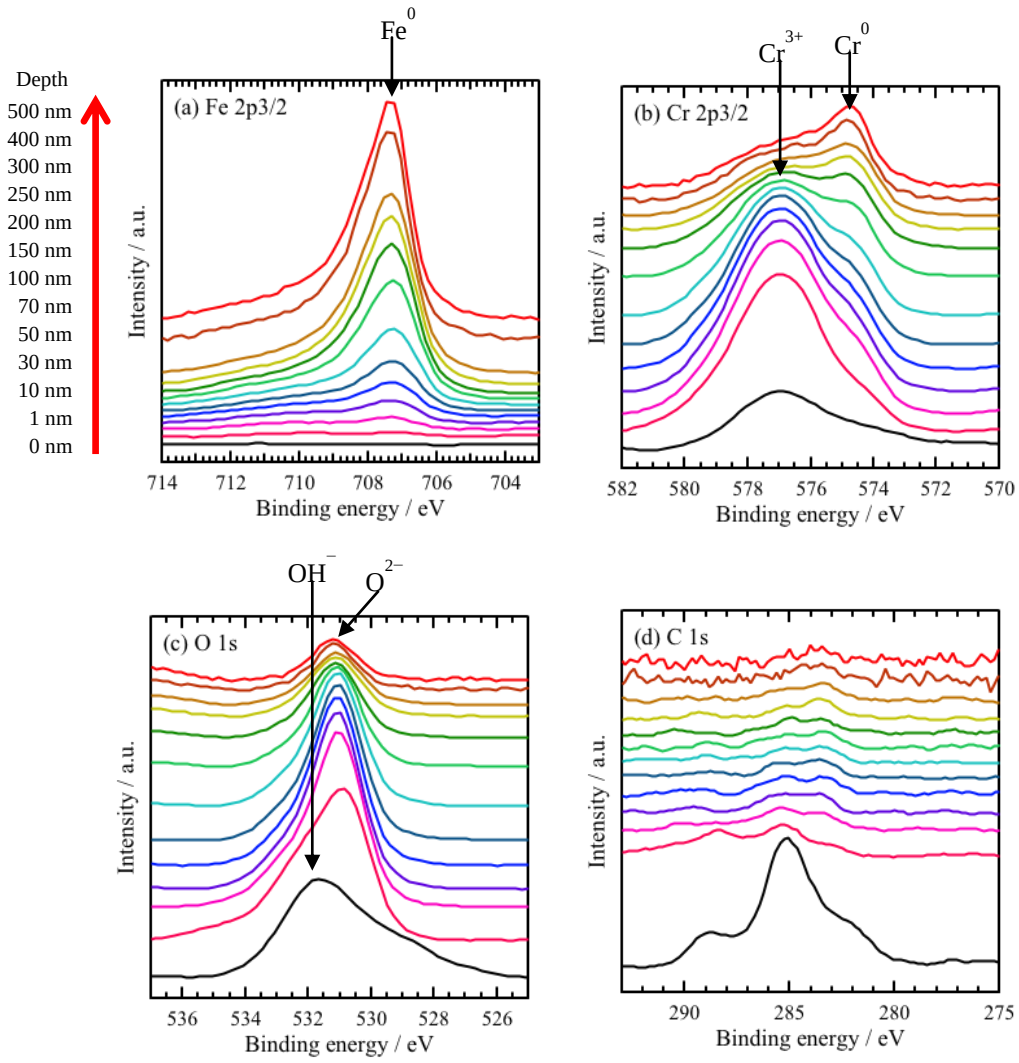

Figure 5. XPS narrow spectra of the sample immersed in 4.0 g/L CH_3COONa solution absence of CO_2 at 353 K for 21.6 ks.

In Figure 5c, the peaks around 532 eV attributed to OH^- [23,25–27] is observed on the surface

(at 0 nm depth). As sputtering, the peaks around 530 eV appear. The peaks are attributed to O^{2-} [23,25–27], and the intensity changed with depth. Form Fe, Cr and O narrow scan spectra, corrosion product layer formed on the steel surface has a double layer structure as an outer layer; Cr hydroxide, and an inner layer; Cr oxide. In Figure 5d, peaks are observed on the surface (at 0 nm depth), and no peak is observed after sputtering. The peaks could not be attributed, however, the result suggests that the CH_3COO^- in the solution may exist only on the surface.

To investigate the composition of sample surface after immersion, a composition ration of Fe and Cr was calculated from XPS narrow scan spectra. Figure 6 shows composition ratio of Fe/Cr as a function of depth. The ratio increases with increasing depth, however, no significant difference with solution composition is observed. These results indicate that the composition ratio of Fe/Cr ratio at the surface is independent of the chemical composition of the used solution and CO_2 bubbling.

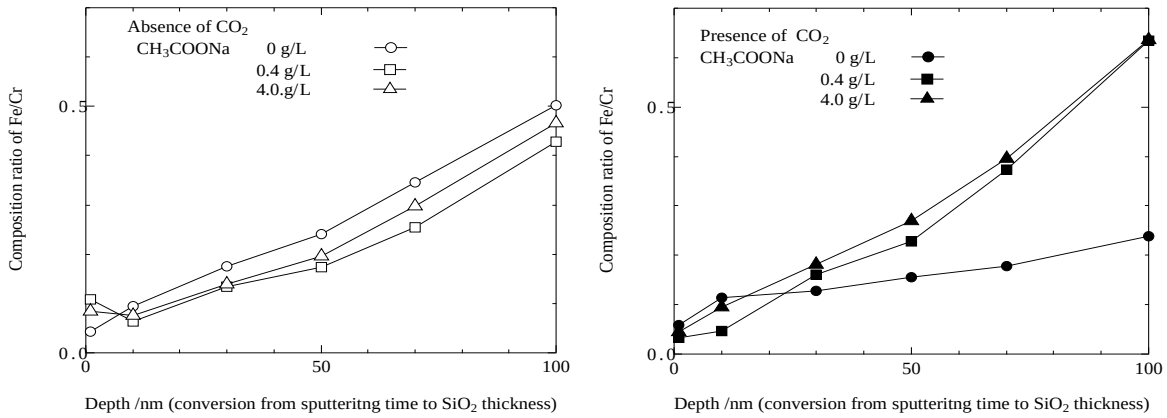

Figure 6. Composition ratio of Fe/Cr obtained from XPS spectra as a function of depth.

3.3. GDS and FT-IR analysis

It is needed to investigate the depth profile of elements in the sample after the immersion tests. GDS was applied to measure the depth profiles of Fe, Cr and O. The depth profile of the sample immersed in 4.0 g/L CH_3COONa solution absence of CO_2 is shown in Figure 7a. The Fe intensity is low at the initial and it increases sharply as sputter time longer than 5 s. The Cr intensity shows a peak about 2 s and a minimum about 5 s. The O intensity shows peak around 1 s and becomes low after 5 s sputtering. These results suggest that the Cr rich layer exists until Cr intensity reached minimum. The sputter time at a minimum of Cr intensity decided from GDS spectra. Figure 7b shows the sputtering time at a minimum of Cr intensity as a function of CH_3COONa concentration. The sputter time at minimum of Cr intensity decreases with increasing CH_3COONa concentration. This result indicates that Cr rich layer becomes thinner with increasing CH_3COONa concentration.

It was suggested that organic substances in the solution adsorbed on the surface from XPS analysis. FT-IR applied to analyze the organic substances on the surface, and obtained spectra are shown in Figure 8. The background spectrum was subtracted to reduce peaks related to CO_2 and H_2O in the environments. However, the residue of CO_2 related peaks are still observed around 2400~2300 cm^{-1} [28,29]. The peaks around 1700~1300 cm^{-1} are attributed to CH_3COO^- or

HCO_3^- [30,31], and the intensity of the peaks increases with increasing CH_3COONa concentration. The intensity obtained in presence of CO_2 shows lager value independent of CH_3COONa concentration. These results indicate that CH_3COO^- or CO_3^{2-} adsorbs on the surfaces.

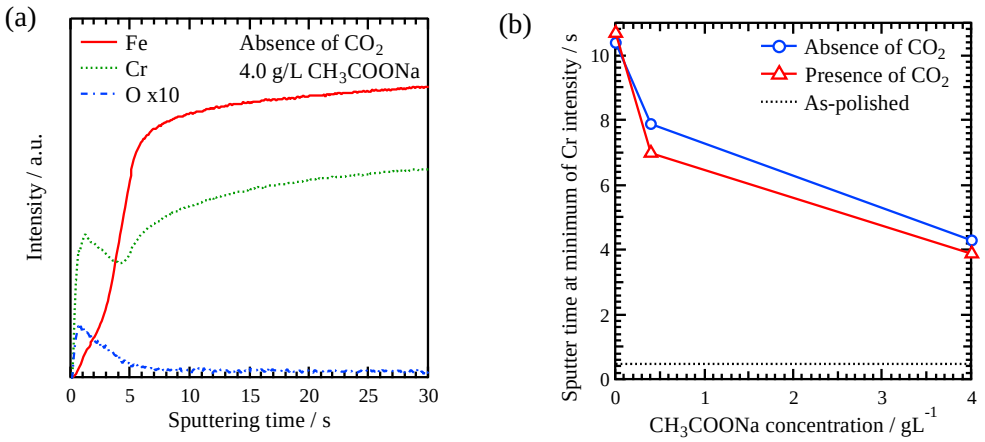

Figure 7. (a) GDS depth profile of the sample immersed in 4.0 g/L CH_3COONa solution absence of CO_2 at 353 K for 21.6 ks. (b) Sputtering time at minimum of Cr intensity as a function of CH_3COONa concentration.

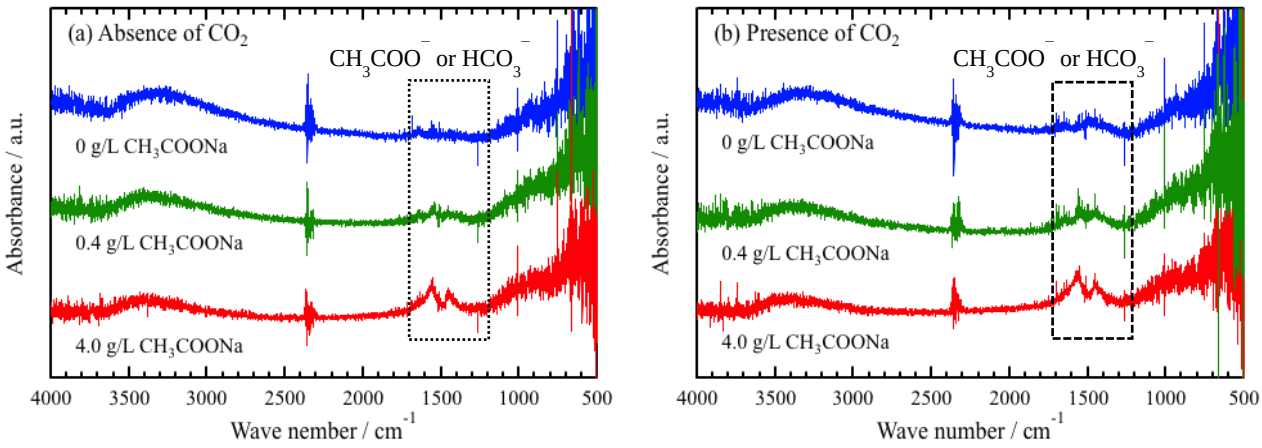

Figure 8. FT-IR spectra of the samples (a) absence of CO_2 and (b) presence of CO_2 after the immersion tests.

3.4. Surface images after immersion corrosion test

Surface morphologies of the samples after 21.6 ks immersion are shown in Figure 9. In Figure 9a,b, uneven surface with dark lines are observed in 0 g/L CH_3COONa. In Figure 9c,d, a small number of dark lines are observed in 0.4 g/L CH_3COONa. However, their size and length are almost the same as observed in 0 g/L CH_3COONa. Smooth surfaces without dark lines are observed in 4.0 g/L CH_3COONa (Figure 9e,f). There are precipitates on the surfaces in all samples, and size and number are changed with CH_3COONa concentration. Little difference of the surface morphology is

observed in the presence and absence of CO_2 in the solutions.

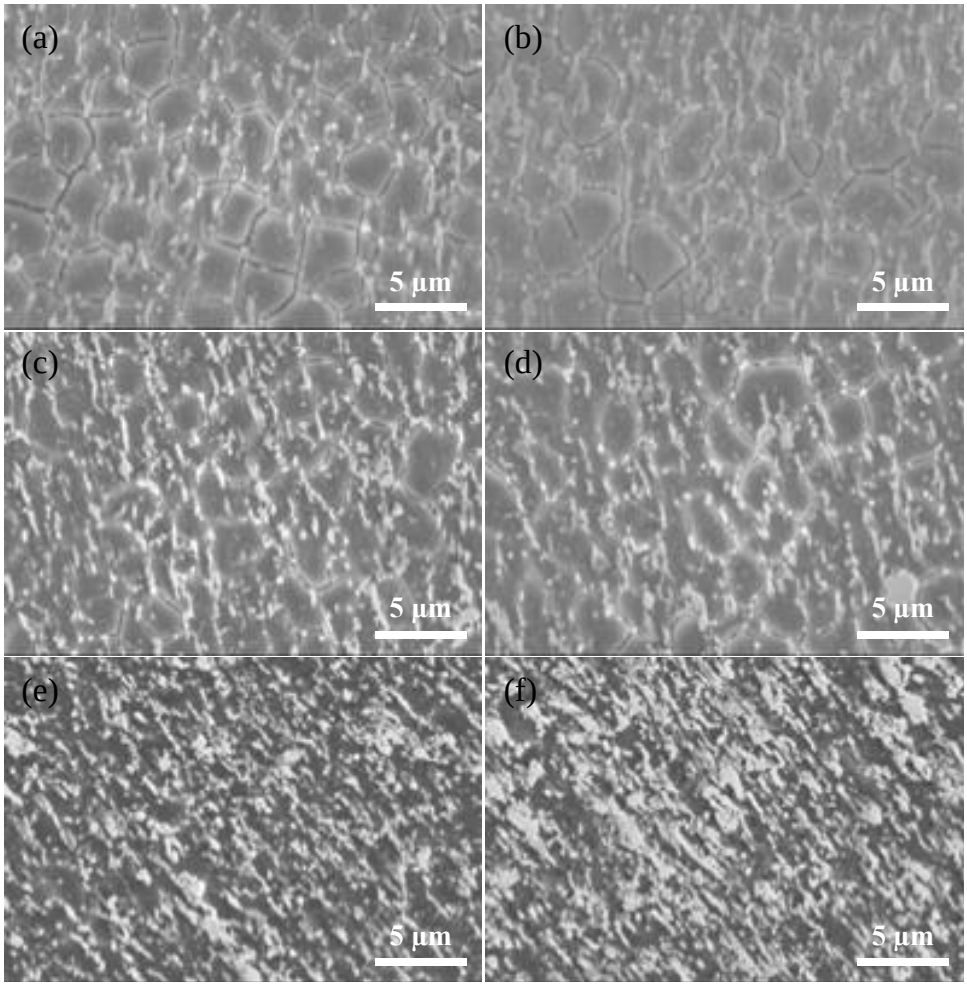

Figure 9. SEM images of the samples after 21.6 ks immersion. (a) and (b) 0 g/L CH_3COONa, (c) and (d) 0.4 g/L CH_3COONa, (e) and (f) 4.0 g/L CH_3COONa. (a), (c) and (e) Absence of CO_2, (b), (d) and (f) Presence of CO_2.

4. Discussion

4.1. Effect of CO_2 gas bubbling

It is known that dissolved CO_2 produced carbonic acid and H^+.

$$CO_2 + H_2O \rightarrow H_2CO_3 \quad (1)$$

$$H_2CO_3 \rightarrow HCO_3^- + H^+ \quad (2)$$

In this experiment, it is considered that the cathodic reaction is the hydrogen evolution reaction because the pH of the used solutions was 3.5. The reaction may change the pH of the solution during polarization measurement. If CO_2 gas flowing during the experiments, Eqs 1 and 2 may occur

continuously and the carbonic acid acts as the source of H^+. Therefore, the pH may be maintained during the polarization tests. This is a possible reason for i_{flat} of 0 g/L CH_3COONa in presence of CO_2 showed the largest value as shown in Figure 3a. The supply of H^+ by Eq 2 in presence of CO_2, make it possible to increase corrosiveness of the solution and may reduce E_{pit} as shown in Figure 3b.

4.2. Effect of CH_3COONa and CO_2 on corrosion process

In this experiment, i_{flat} decreased with increasing concentration of CH_3COONa, while a small difference in surface composition was observed by surface analysis. The thickness of the Cr rich layer changed with the concentration of CH_3COONa that was observed by GDS, and the adsorptions of CH_3COO^- or HCO_3^- on the surface were observed by FT-IR. These results may closely relate to corrosion process. Schematic representation of the corrosion process in these experimental conditions is shown in Figure 10. A highly protective layer is formed on the steel surface when the absence of CH_3COONa and CO_2 in the solution (Figure 10a). The corrosion is progressed by Cl^-. The Cr rich layer is formed on the surface because of preferential Fe dissolution [32,33]. The thickness of the Cr rich layer may become thicker and then reaches a certain value as metal dissolution. In the case of CH_3COONa and CO_2 are present in the solutions, CH_3COO^- and HCO_3^- adsorb on the steel surface (Figure 10b). The absorbed layer may inhibit the dissolution of metals, therefore, the amount of dissolved metals decreases and relatively thin Cr rich layer is formed.

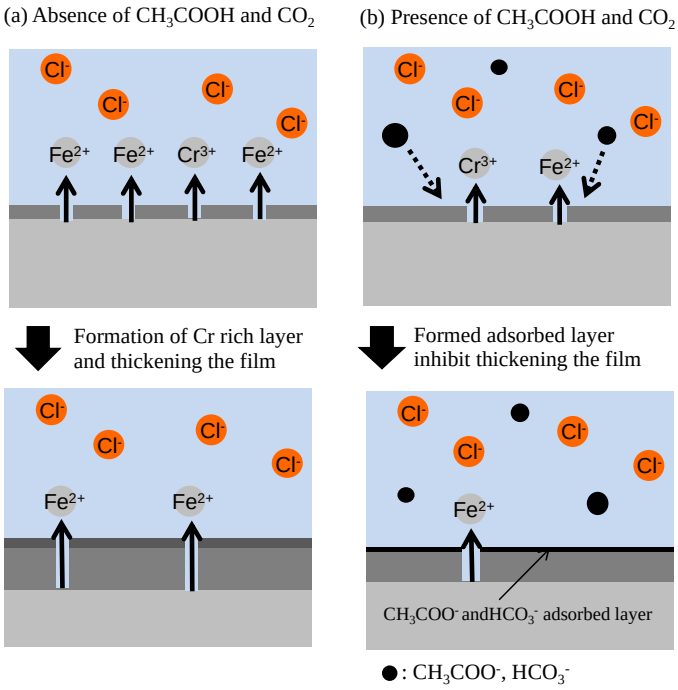

Figure 10. Schematic representation of the corrosion process in these experimental conditions.

5. Conclusion

The influences of CH_3COONa and CO_2 on the corrosion behavior of 13 mass% Cr martensitic

steels in simulated oil and gas environments were investigated with electrochemical and surface analysis techniques. Following conclusions may be drawn:

(1) There was the plateau region of the current density, i_{flat}, in the anodic polarization curves, and the i_{flat} decreased with increasing CH_3COONa concentration. In the case of the solutions with CH_3COONa, little effect of CO_2 on the i_{flat} was observed. A pitting potential, E_{pit} shifted to the positive direction as increasing CH_3COONa concentration, and showed the negative value by adding CO_2.

(2) The Cr enriched layer formed on the surface of the sample after the immersion test, and the thickness of the layer became thinner as increasing CH_3COONa concentration. The adsorbed CH_3COO^- and HCO_3^- on the sample surfaces prevented the corrosion.

Acknowledgements

An observation of SEM was conducted at the Laboratory of XPS analysis, Joint-use facilities, Hokkaido University, supported by Material Analysis and Structure Analysis Open Unit (MASAOU). XPS analysis was conducted at the Laboratory of XPS analysis, Joint-use facilities, Hokkaido University, supported by 'Nanotechnology Platform' Program of the Ministry of Education, Culture, Sports, Science and Technology (MEXT), Japan.

Conflict of interest

All authors have no conflict of interest directly relevant to the contents of this article.

References

1. Masamura K, Hashizume S, Sakai J, et al. (1987) Polarization behavior of high-alloy OCTG in CO_2 environment as affected by chlorides and sulfides. *Corrosion* 43: 359–365.
2. Kimura M, Miyata Y, Yamane Y, et al. (1999) Corrosion resistance of high-strength modified 13% Cr steel. *Corrosion* 55: 756–761.
3. Guo XP, Tomoe Y (1998) Electrochemical behavior of carbon steel in carbon dioxide-saturated diglycolamine solutions. *Corrosion* 54: 931–939.
4. Kimura M, Miyata Y, Toyooka T, et al. (2001) Effect of retained austenite on corrosion performance for modified 13% Cr steel pipe. *Corrosion* 57: 433–439.
5. Turnbull A, Griffiths A (2003) *Review*: Corrosion and cracking of weldable 13 wt-%Cr martensitic stainless steels for application in the oil and gas industry. *Corros Eng Sci Techn* 38: 21–50.
6. Anselmo N, May JE, Mariano NA, et al. (2006) Corrosion behavior of supermartensitic stainless steel in aerated and CO_2-saturated synthetic seawater. *Mat Sci Eng A-Struct* 428: 73–79.
7. Sunaba T, Meng H, Tomoe Y, et al. (2009) Corrosion experience of 13%Cr steel tubing and laboratory evaluation of super 13Cr steel in sweet environments containing acetic acid and trace amounts of H_2S. *Corrosion 2009*, NACE International, NACE-09568.

8. Sunaba T, Ito T, Miyata Y, et al. (2014) Influence of chloride ions on corrosion of modified martensitic stainless steels at high temperatures under a CO_2 environment. *Corrosion* 70: 988–999.
9. Liu D, Qiu YB, Tomoe Y, et al. (2011) Interaction of inhibitors with corrosion scale formed on N80 steel in CO_2-saturated NaCl solution. *Mater Corros* 62: 1153–1158.
10. Zhang Y, Pang X, Qu S, et al. (2012) Discussion of the CO_2 corrosion mechanism between low partial pressure and supercritical condition. *Corros Sci* 59: 186–197.
11. Liu QY, Mao LJ, Zhou SW (2014) Effects of chloride content on CO_2 corrosion of carbon steel in simulated oil and gas well environments. *Corros Sci* 84: 165–171.
12. Islam MA, Farhat ZN (2013) The synergistic effect between erosion and corrosion of API pipeline in CO_2 and saline medium. *Tribol Int* 68: 26–34.
13. Hashizume S, Minami Y, Ishizawa Y (1998) Corrosion resistance of martensitic stainless steels in environments simulating carbon dioxide gas wells. *Corrosion* 54: 1003–1011.
14. Hashizume S, Nakayama T, Sakairi M, et al. (2008) Electrochemical behavior of low C-13%Cr weld joints by using solution flow type micro-droplet cell. *Corrosion 2018*, NACE International, NACE-08102.
15. Hashizume S, Nakayama T, Sakairi M, et al. (2009) Effect of PWHT on electrochemical behavior of low C-13%Cr welded joints with the use of a solution flow type micro-droplet cell. *Corrosion 2009*, NACE International, NACE-09089.
16. Sakairi M, Nakayama T, Kikuchi T, et al. (2009) Electrochemical noise analysis of 13 mass% Cr stainless steel HAZ by solution flow type micro-droplet cell-Effect of solution concentration-. *ECS Trans* 16: 281–290.
17. Hashizume S, Nakayama T, Sakairi M, et al. (2011) SCC mechanism near fusion line of low C-13%Cr welded joints. *Zairyo-to-Kankyo* 60: 196–201.
18. Sakairi M, Kikawa A, Hashizume S, et al. (2013) Effect of sodium acetate in model oil and gas environments on oxide film structure and corrosion behavior of 13%Cr stainless steel. *Proceedings of NACE International East Asia and Pacific Rim Area Conference and Expo 2013*, Kyoto, EPA13-4605.
19. Fierro G, Ingo GM, Mancia F (1989) XPS investigation on the corrosion behavior of 13Cr-martensitic stainless steel in CO_2-H_2S-Cl^- environments. *Corrosion* 45: 814–823.
20. Fierro G, Ingo GM, Mancia F, et al. (1990) XPS investigation on AISI 420 stainless steel corrosion in oil and gas well environments. *J Mater Sci* 25: 1407–1415.
21. Islam MA, Farhat ZN (2015) Characterization of the corrosion layer on pipeline steel in sweet environment. *J Mater Eng Perform* 24: 3142–3158.
22. Nicic I, Macdonald DD (2008) The passivity of Type 316L stainless steel in borate buffer solution. *J Nucl Mater* 379: 54–58.
23. Ikeo N, Iijima Y, Niimura N, et al. (1991) *Handbook of X-Ray photoelectron spectroscopy*, Tokyo, Japan: JEOL Ltd.
24. Descostes M, Mercier F, Thromat N, et al. (2000) Use of XPS in the determination of chemical environment and oxidation state of iron and sulfur samples: constitution of a data basis in binding energies for Fe and S reference compounds and applications to the evidence of surface species of an oxidized pyrite in a carbonate medium. *Appl Surf Sci* 165: 288–302.

25. Jung RH, Tsuchiya H, Fujimoto S (2012) XPS characterization of passive films formed on Type 304 stainless steel in humid atmosphere. *Corros Sci* 58: 62–68.
26. Yin ZF, Wang XZ, Liu L, et al. (2011) Characterization of corrosion product layers from CO_2 corrosion of 13Cr stainless steel in simulated oilfield solution. *J Mater Eng Perform* 20: 1330–1335.
27. Zhang J, Wang ZL, Wang ZM, et al. (2012) Chemical analysis of the initial corrosion layer on pipeline steels in simulated CO_2-enhanced oil recovery brines. *Corros Sci* 65: 397–404.
28. Ramis G, Busca G, Lorenzelli V (1991) Low-temperature CO_2 adsorption on metal oxides: spectroscopic characterization of some weakly adsorbed species. *Mater Chem Phys* 29: 425–435.
29. Hiyoshi N, Yoga K, Yashima T (2005) Adsorption of carbon dioxide on aminosilane-modified mesoporous silica. *J Jpn Petrol Inst* 48: 20–36.
30. Yoshida H, Adachi Y, Kamegawa K (1982) Fourier transform infrared spectra of activated carbons. *Tanso* 111: 149–153.
31. Geng W, Nakajima T, Takanashi H, et al. (2009) Analysis of carboxyl group in coal and coal aromaticity by Fourier transform infrared (FT-IR) spectrometry. *Fuel* 88: 139–144.
32. Maurice V, Yang WP, Marcus P (1998) X-ray photoelectron spectroscopy and scanning tunneling microscopy study of passive films formed on (100) Fe–18Cr–13Ni single-crystal surfaces. *J Electrochem Soc* 145: 909–920.
33. Tardio S, Abel ML, Carr RH, et al. (2015) Comparative study of the native oxide on 316L stainless steel by XPS and ToF-SIMS. *J Vac Sci Technol A* 33: 05E122.

AIMS Press